International Journal of Mathematical Analysis and Modelling

(Formerly Journal of the Nigerian Society for Mathematical Biology)

Volume 8 Issue 1, 2025

ISSN (Print): 2682 - 5694
ISSN (Online): 2682 – 5708
www.tnsmb.org

Transient sensitivity and Monte Carlo spectral analysis in stage-structured manufacturing systems

I.J. Ugbene *†and I.B. Tejere†‡

Abstract

This study presents a mathematical modeling and simulation scheme for optimizing multi-stage production systems with dormancy effects, transition dynamics, and rework mechanisms. A staged structured approach is employed to capture the interplay between production flow, storage capacities, and material recovery. Sensitivity and elasticity analyses are conducted to evaluate the impact of transition rates on total production output. The results indicate that an increase in transition rate γ_2 significantly enhances production efficiency, as demonstrated by a sensitivity of 1007.36 and an elasticity of 5.44. However, an unregulated increase in transition rates can create bottlenecks in downstream stages, necessitating capacity adjustments and strategic control measures. The study concludes that a balanced optimization of transition dynamics, dormancy effects, and storage capacities is critical for enhancing overall system efficiency. Future work will focus on integrating stochastic optimization techniques and adaptive control strategies to refine decision-making in real-time manufacturing systems.

Keywords and phrases: multi-stage production; dormancy effects; transition rates; sensitivity analysis; elasticity; stage structured model; optimization.

1 Introduction

Manufacturing systems are complex and dynamic, requiring robust modeling techniques to capture their transient behaviors, uncertainties, and feedback loops. Traditional models, such as Markov chains and basic transition matrices, have been widely used but often fall short in representing backward transitions caused by quality control failures, machine breakdowns, and rework processes. The doubly Lefkovitch matrix model [1, 2], an extension of the Lefkovitch matrix, addresses these shortcomings by incorporating both forward and backward transitions, making it particularly well-suited for systems involving iterative quality control, recycling, or repair processes [3, 4]. Unlike the classical Lefkovitch model, which assumes unidirectional movement through discrete production states, the doubly Lefkovitch framework captures the more realistic, non-monotonic transitions often seen in modern manufacturing lines [5, 6].To further enrich the modeling landscape, insights from biological Boolean networks [7–10] can be leveraged to understand discrete decision-making processes and regulatory logic in manufacturing workflows. These networks [11–13], originally developed to describe gene regulatory systems, offer a formalism for encoding binary states and logical transitions across a complex network of interacting components, which closely parallels fault detection, machine states, and process control in smart manufacturing systems. Additionally, transformation semigroup theory [14–16] provides an algebraic framework to analyze the compositional structure of state transitions within such systems. By representing process dynamics as semigroup actions [17, 18] on finite state spaces, it becomes possible to study the system's behavior under repeated operations, uncovering fixed points, cycles, and reachability properties essential for both optimization and resilience analysis.

*Corresponding Author; E-mail: ugbene.ifeanyi@fupre.edu.ng
†Department of Mathematics, Federal University of Petroleum Resources, Effurun, Nigeria.
‡E-mail: ifeanyichukwublessing15@gmail.com

Sensitivity analysis plays a critical role in understanding how small variations in system parameters influence overall efficiency. While conventional sensitivity analyses focus on steady-state behaviors, transient sensitivity analysis is essential for identifying short-term variations and early-stage failures [19,]. This method is particularly useful in assessing how variations in defect rates, machine reliability, or supply chain fluctuations impact production efficiency [21, 22]. For example, defects in an automated assembly line may require products to return to earlier stages for rework, significantly affecting throughput [23, 24]. Similarly, fluctuating demand may necessitate adaptive inventory management, where transient sensitivity analysis helps identify optimal stock levels under uncertain conditions [25]. By incorporating transient sensitivity analysis within the doubly Lefkovitch framework, manufacturers can optimize rework loops, prevent bottlenecks, and improve response strategies to production disruptions [26, 27].

Monte Carlo spectral analysis further enhances system optimization by modeling stochastic variations and uncertainties [28, 29]. This method generates probabilistic simulations to evaluate system performance under variable conditions, making it valuable for predicting failure rates, optimizing quality control, and assessing production risks [30, 31]. Monte Carlo techniques are particularly useful when analyzing manufacturing environments with random fluctuations in demand, supply delays, or equipment failures [32, 33]. For example, in a robotic manufacturing system, variations in sensor precision or machine speed can lead to unexpected downtimes, which Monte Carlo simulations help mitigate [34, 35]. Furthermore, this analysis assists in developing contingency strategies for minimizing defects and optimizing resource allocation [36, 37]. Integrating transient sensitivity analysis and Monte Carlo spectral analysis within the doubly Lefkovitch framework offers a powerful approach to improving manufacturing resilience and efficiency. This combination allows manufacturers to anticipate production instabilities, adjust processes dynamically, and enhance decision-making under uncertainty [38–40]. As modern manufacturing systems become increasingly complex, leveraging these analytical tools can significantly reduce waste, improve production output, and optimize system performance [41–43]. Future research should focus on applying these methodologies to real-world case studies while integrating machine learning techniques for enhanced predictive modeling and automation.

2 Materials and method

The manufacturing process is structured into six stages: raw materials, processing, assembly, quality inspection, packaging, and distribution. The population of items at each stage is represented by the vector $X(t)$, where

$$X(t) = \begin{bmatrix} X_1(t) \\ X_2(t) \\ X_3(t) \\ X_4(t) \\ X_5(t) \\ X_6(t) \end{bmatrix} \tag{1}$$

Each $X_i(t)$ represents the number of items in stage i at time t. The transitions between stages are governed by the time-dependent doubly Lefkovitch matrix $L(t)$, which is generally defined as

$$L = \begin{pmatrix} d_1 & a_1 & a_2 & \cdots & a_{n-2} & a_{n-1} \\ b_1 & d_2 & 0 & \cdots & 0 & c_{n-2} \\ 0 & b_2 & d_3 & \ddots & \vdots & \vdots \\ \vdots & \ddots & \ddots & \ddots & 0 & c_2 \\ \vdots & & \ddots & b_{n-2} & d_{n-1} & c_1 \\ 0 & \cdots & \cdots & 0 & b_{n-1} & d_n \end{pmatrix} \tag{2}$$

with $0 < b_i \leq 1$, $a_j \geq 0$, $i, j = 1, 2, \ldots, n-1$, $d_k \geq 0$, $k = 1, 2, \ldots, n$, and $c_i \geq 0$, $i = 1, 2, \ldots, n-2$, where not all are zeros. Particularly considering the six manufacturing processes, we get;

$$L(t) = \begin{bmatrix} d_1(t) & a_1(t) & a_2(t) & a_3(t) & a_4(t) & a_5(t) \\ b_1(t) & d_2(t) & 0 & 0 & 0 & c_4(t) \\ 0 & b_2(t) & d_3(t) & 0 & 0 & c_3(t) \\ 0 & 0 & b_3(t) & d_4(t) & 0 & c_2(t) \\ 0 & 0 & 0 & b_4(t) & d_5(t) & c_1(t) \\ 0 & 0 & 0 & 0 & b_5(t) & d_6(t) \end{bmatrix} \tag{3}$$

The system dynamics follow the equation

$$X(t+1) = L(t)X(t)$$

where $b_i(t)$ represents the transition rates from stage i to $i+1$, $d_i(t)$ represents the dormancy rates, $c_i(t)$ denotes the fraction of items returning for rework, and $a_i(t)$ represents recycling flows back to the raw materials stage. In this model, the parameters $a_1(t)$, $a_2(t)$, and $a_3(t)$ are set to zero because

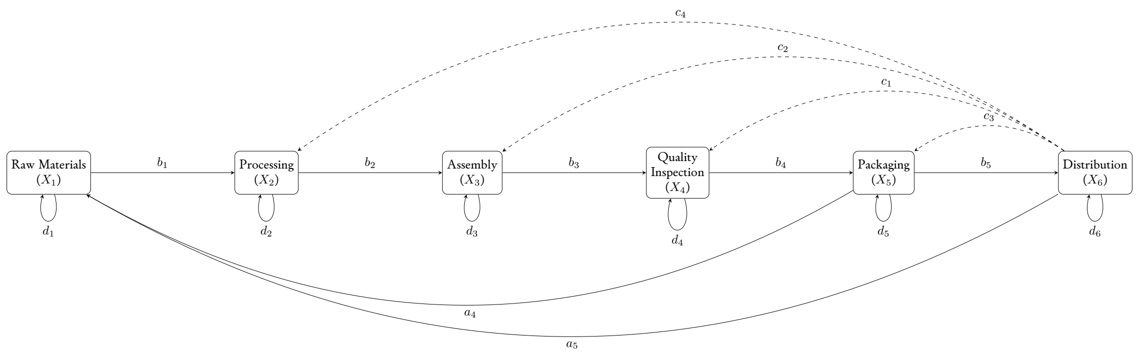

Figure 1: Manufacturing Process Flow Diagram

they are not relevant to the manufacturing process.

By including deterministic functions that specifically take into consideration important system factors like production volumes, resource availability, and operational efficiency, the model depicts stage-specific interactions in manufacturing. A organized flow of resources and products is ensured by these functions, which control transitions between crucial manufacturing phases, raw material processing, assembly, quality control, packaging, and distribution. The following are the governing equations:

An **inverse logistic function** of the stage population, $X_i(t)$, provides the dormancy rate $d_i(t)$, which characterizes the duration of time spent in stage i:

$$d_i(t) = \frac{\alpha_i}{1 + \beta_i X_i(t)}, \tag{4}$$

where the inherent dormancy rate under low occupancy is represented by $\alpha_i \in (0, 1)$ and the rate of decrease is regulated by $\beta_i > 0$ while $X_i(t)$ grows. When tiny $X_i(t)$ is detected, dormancy takes the value of α_i, but high occupancy causes dormancy to be inhibited because of retention constraints or throughput prioritization.

The transition rate $b_i(t)$ describes the migration from stage i to $i+1$ and, like the shift between stages, is characterized by a rational function that is constrained by the carrying capacity K_i:

$$b_i(t) = \gamma_i \left(1 - \frac{X_i(t)}{K_i}\right), \tag{5}$$

where $\gamma_i \in (0,1)$ be the maximum rate of growth under optimal circumstances. However, congestion slows transitions as $X_i(t)$ approaches its limit K_i, which reflects constraints in equipment capacity or workforce availability.

The limits of reprocessing capacity are captured by the saturation function of the rework rate $c_i(t)$, which takes into account defective items sent back to earlier stages:

$$c_i(t) = \delta_i \frac{X_i(t)}{1 + X_i(t)}, \tag{6}$$

where, the maximal defect rate is $\delta_i \in (0,1)$. While bigger populations call for quality-control actions, hence reducing defect propagation, modest $X_i(t)$ returns scale linearly with $X_i(t)$.

Redirecting objects to raw materials, the material recovery rate $a_i(t)$, follows a Michaelis-Menten-like form.

$$a_i(t) = \eta_i \frac{X_i(t)}{K_i + X_i(t)}, \tag{7}$$

with $\eta_i \in (0,1)$ as the best cycling efficiency. Fixed processing costs cause inefficiencies in recovery at low $X_i(t)$ increases, economies of scale enhance material reuse.

The dominating eigenvalue $\lambda_{\max}$ of $L(t)$ defines the system's stability. This variable controls whether over time production increases, stabilizes, or decreases. The system goes unstable if $\lambda_{\max} > 1$. Growing exponentially, output results in overabundance, surplus inventory, and possible resource shortages. It comes to equilibrium if $\lambda_{\max} = 1$. Raw inputs and outputs, that is, distributed goods, balance exactly to sustain constant production free from waste or shortages. Production contracts with time if $\lambda_{\max} < 1$. Insufficient output, supply chains broken, and unfulfilled demand follow from this fall-off. Manufacturers can modify matrix progression, regression, or stasis rates by examining $\lambda_{\max}$, therefore stabilizing output and preventing inefficiencies.

2.1 Monte Carlo method

Monte Carlo simulations are performed to analyze the effect of stochastic variations on the transition parameters. In these simulations, realizations of $L(t)$ are generated and the system is solved iteratively over multiple runs to determine expected trends in production stability, efficiency, and waste minimization. Numerical approaches based on Monte Carlo principles for eigenvalue estimation generally fall into two categories: direct computation techniques and successive approximation procedures [44]. Here we focus on stationary linear iterative algorithms derived from Monte Carlo principles for spectral value determination.

Consider an invertible matrix $A \in \mathbb{R}^{n\times n}$ that possesses a complete eigenbasis $X = [\boldsymbol{x}_1|\cdots|\boldsymbol{x}_n]$ such that

$$X^{-1}AX = \text{diag}(\lambda_1, \ldots, \lambda_n), \tag{8}$$

with spectral radii satisfying $|\lambda_1| > |\lambda_2| \geq \cdots \geq |\lambda_n|$. A fundamental iterative scheme to approximate the dominant eigenvalue λ_1 generates vector sequences via the recursion

$$\boldsymbol{y}^{(k)} = A\boldsymbol{f}^{(k-1)} \tag{9}$$

$$\boldsymbol{f}^{(k)} = \frac{\boldsymbol{y}^{(k)}}{\|\boldsymbol{y}^{(k)}\|_2} \tag{10}$$

$$\lambda^{(k)} = [\boldsymbol{f}^{(k)}]^\top A\boldsymbol{f}^{(k)} \quad (k = 1, 2, \ldots) \tag{11}$$

This procedure converges linearly to λ_1 with asymptotic error behavior characterized by

$$|\lambda_1 - \lambda^{(k)}| = \mathcal{O}\left(\left|\frac{\lambda_2}{\lambda_1}\right|^k\right), \tag{12}$$

provided that the initial vector $\boldsymbol{f}^{(0)}$ has a non-negligible projection onto the principal eigen-direction.

To compute non-dominant eigenvalues, the fundamental algorithm requires transformation. One approach is spectral translation, where one defines the modified operator as $P = A - \phi I$, with ϕ as a spectral offset parameter; this shifted formulation enables convergence to $\lambda_i - \phi$. Alternatively, an inverse transformation $P = A^{-1}$ (valid when A is nonsingular) converts minimal eigenvalues to dominant positions. A composite modification $P = (A - \phi I)^{-1}$ combines spectral translation and inversion, allowing targeted convergence to specific eigenvalues near ϕ. This transformed operator P preserves the original eigenbasis while altering the spectral magnitude ordering, permitting flexible eigenvalue isolation through appropriate parameter selection and algebraic manipulation.

Within a stochastic computational framework for spectral analysis, consider a real square matrix $A = [a_{ij}]_{i,j=1}^{n} \in \mathbb{R}^{n\times n}$ paired with column vectors $\mathbf{b} = (b_1, \dots, b_n)^\top$ and $\mathbf{h} = (h_1, \dots, h_n)^\top$. The matrix-vector product $A\mathbf{b}$ serves as the computational cornerstone for iterative stochastic algorithms. In this context, one analyzes a discrete-time Markov process with state transitions

$$s_0 \to s_1 \to \cdots \to s_k \tag{13}$$

where each state $s_j \in \{1, \dots, n\}$ for $0 \le j < k$, terminating at an absorbing state $s_k = n + 1$. The transition kernel $P = [p_{ij}]$ governs probabilistic movements among the $n + 1$ states, with p_{ij} representing the likelihood of transitioning from state i to j.

For a given stochastic path $\gamma = (s_0, s_1, \dots, s_m, n + 1)$ starting from $s_0 < n + 1$, traversing intermediate states $(s_1, \dots, s_m)$ and terminating at the absorbing state, let $\mathbf{a} = (a_1, \dots, a_n)$ denote the initial state distribution (with $\sum_{i=1}^{n} a_i = 1$). The probability of the path is computed as

$$\mathbb{P}(\gamma) = a_{s_0} \prod_{t=0}^{m-1} p_{s_t s_{t+1}} \cdot p_{s_m(n+1)} \tag{14}$$

Within this trajectory space, one defines estimator classes for solution components x_i by

$$\Theta_i(\gamma) = W_m(\gamma) \frac{\delta_{i s_m}}{p_{s_{m-1} s_m}}, \quad \Lambda_i(\gamma) = \sum_{t=0}^{m} W_t(\gamma) \delta_{i s_t}, \tag{15}$$

where δ_{ij} is the Kronecker delta. The weighting factors $\{W_t\}$ evolve recursively as

$$W_0(\gamma) = \frac{c_{s_0} a_{s_0}}{a_{s_0}}, \quad W_t(\gamma) = W_{t-1} \frac{a_{s_t}}{p_{s_{t-1} s_t}} = c_{s_0} \prod_{r=1}^{t} \frac{a_{s_r}}{p_{s_{r-1} s_r}}, \tag{16}$$

ensuring that the estimators are unbiased:

$$\mathbb{E}[\Theta_i] = \mathbb{E}[\Lambda_i] = x_i, \quad \forall i \in \{1, \dots, n\}. \tag{17}$$

The configuration of the Markov chain is defined by the initial state probability

$$\mathbb{P}(s_0 = \alpha) = \frac{|h_\alpha|}{\sum_{\beta=1}^{n} |h_\beta|} \tag{18}$$

and the transition probability

$$\mathbb{P}(s_t = \beta | s_{t-1} = \alpha) = \frac{|a_{\alpha\beta}|}{\sum_{\gamma=1}^{n} |a_{\alpha\gamma}|}, \quad \alpha \in \{1, \dots, n\} \tag{19}$$

These probabilities form the basis for constructing the weighted estimators, where the evolution of stochastic weights follows

$$W_0 = \frac{h_{s_0}}{\mathbb{P}(s_0)}, \quad W_t = W_{t-1} \frac{a_{s_{t-1} s_t}}{\mathbb{P}(s_t | s_{t-1})} \tag{20}$$

and one has

$$\mathbb{E}[W_t f_{s_t}] = (\mathbf{h}, A^t \mathbf{f}).$$

Dominant eigenvalue estimation is achieved through ratio estimators. For large i, one approximates the spectral radius $\lambda_{\max}$ as

$$\begin{aligned}\lambda_{\max} &\approx \frac{\mathbb{E}[W_i f_{s_i}]}{\mathbb{E}[W_{i-1} f_{s_{i-1}}]} \\ &\approx \frac{\frac{1}{N}\sum_{\nu=1}^{N} W_i^{(\nu)} f_{s_i^{(\nu)}}}{\frac{1}{N}\sum_{\nu=1}^{N} W_{i-1}^{(\nu)} f_{s_{i-1}^{(\nu)}}}\end{aligned} \tag{21}$$

where the superscript (ν) indexes N independent realizations. This formulation leverages ergodic averages over Monte Carlo trials to statistically approximate spectral properties.

Furthermore, spectral radius estimation can be approached via operator series expansion. Let $\rho_{\max}$ denote the spectral radius of the non-negative matrix $\widetilde{A} = [|a_{ij}|]$. Under the condition $|\rho_{\max}\phi| < 1$ for a chosen parameter ϕ, the following operator series identity holds:

$$\langle (I - \phi A)^{-m}\mathbf{f}, \mathbf{h}\rangle = \mathbb{E}\left[\sum_{k=0}^{\infty} \phi^k \binom{k+m-1}{m-1} W_k f(x_k)\right] \tag{22}$$

The Neumann series expansion

$$(I - \phi A)^{-m} = \sum_{k=0}^{\infty} \binom{k+m-1}{m-1} \phi^k A^k$$

converges uniformly under the spectral radius condition, and applying this expansion to an arbitrary vector $\mathbf{f}$ yields

$$\langle (I - \phi A)^{-m}\mathbf{f}, \mathbf{h}\rangle = \mathbb{E}\left[\sum_{k=0}^{\infty} \phi^k \binom{k+m-1}{m-1} \langle A^k \mathbf{f}, \mathbf{h}\rangle\right] \tag{23}$$

Absolute convergence under $|\rho_{\max}\phi| < 1$ justifies term-wise averaging via Fubini's theorem.

The smallest magnitude eigenvalue $\lambda_{\min}$ can be estimated using the relation

$$\begin{aligned}\lambda_{\min} \approx \frac{1}{\phi}\left(1 - \frac{1}{\mu^{(m)}}\right) &= \frac{\langle A(I - \phi A)^{-m}\mathbf{f}, \mathbf{h}\rangle}{\phi \sum_{k=1}^{\infty} \mu^{(m)} c_{k-1} \langle (I - \phi A)^{-m}\mathbf{f}, \mathbf{h}\rangle} \\ &= \frac{\mathbb{E}\left[\sum_{k=1}^{\infty} \phi^k \binom{k+m-1}{m-1} W_k f(x_k)\right]}{\mathbb{E}\left[\sum_{k=0}^{\infty} \phi^k \binom{k+m-1}{m-1} W_{k+1} f(x_{k+1})\right]} \\ &= \frac{\mathbb{E}\left[\sum_{k=0}^{\infty} \phi^k \binom{k+m-1}{m-1} W_k f(x_k)\right]}{\mathbb{E}\left[\sum_{k=0}^{\infty} \phi^k \binom{k+m-1}{m-1} W_k f(x_k)\right]}\end{aligned} \tag{24}$$

where the weighting functions $\{W_k\}$ follow the recursive definition provided earlier.

Finally, a parameter optimization strategy is employed where the shift parameter $\phi < 0$ is chosen to minimize the convergence factor

$$\mathcal{L}(\phi, A) = \frac{1 + |\phi|\widetilde{\lambda}_1}{1 + |\phi|\widetilde{\lambda}_2},$$

with $\widetilde{\lambda}_1$ and $\widetilde{\lambda}_2$ denoting the ordered eigenvalues of $\widetilde{A}$. For systems where the spectral ratio satisfies $\widetilde{\lambda}_1 = \alpha\widetilde{\lambda}_2$ (with $0 < \alpha < 1$), this becomes

$$\mathcal{L}(\phi, A) = 1 - \frac{|\phi|\widetilde{\lambda}_2(1-\alpha)}{1 + |\phi|\widetilde{\lambda}_2}. \tag{25}$$

In practical implementations, a baseline choice might be $\phi = -\frac{1}{2\|A\|}$, with adaptive tuning following $\phi = -\frac{\alpha}{\|A\|}$ (for $0 < \alpha < 1$), optimized through Monte Carlo trials.

2.2 Transient Sensitivity

To analyze how perturbations in the parameters of $L(t)$ affect the evolution of the system, we apply transient sensitivity analysis. Following methodologies developed for structured population models, the transient sensitivity of the population vector to a change in an element of the projection matrix can be decomposed into contributions arising from the equilibrium configuration and deviations from it [45]. In the context of our manufacturing model, if we consider a perturbation in a parameter, say, a change in one of the recycling flows $a_i(t)$ or transition rates $b_i(t)$—the corresponding sensitivity of $X(t)$ can be expressed analogously to

$$\frac{\partial X(t)}{\partial l_{ij}(t)} = \mathcal{G}_s(t, l_{ij}(t))\frac{X(0)}{\|u^{(1)}\|} + \mathcal{G}_d(t, l_{ij}(t))L(t)X(t), \tag{26}$$

where $l_{ij}(t)$ is a representative element of $L(t)$, $u^{(1)}$ is the dominant right eigenvector of $L(t)$, and the operators $\mathcal{G}_s$ and $\mathcal{G}_d$ capture the equilibrium and deviation contributions respectively.

In a more general setting, the transient sensitivity of the demographic vector $\boldsymbol{\eta}(t)$ (here corresponding to the stage-wise item counts) to perturbations in a matrix element a_{ij} of a projection operator $\boldsymbol{\mathcal{A}}$ is given by

$$\frac{\partial \boldsymbol{\eta}(t)}{\partial a_{ij}} = \underbrace{\boldsymbol{\mathcal{G}}_s(t, a_{ij})\frac{\boldsymbol{\eta}(0)}{\|\boldsymbol{u}^{(1)}\|}}_{\text{Invariant to initial population structure}} + \underbrace{\boldsymbol{\mathcal{G}}_d(t, a_{ij})\boldsymbol{\mathcal{A}}\boldsymbol{\eta}}_{\text{Linearly influenced by initial conditions}} \tag{27}$$

with the divergence from equilibrium defined as

$$\boldsymbol{\eta}_{\Delta} = \boldsymbol{\eta}(0) - \frac{\langle \boldsymbol{v}^{(1)}, \boldsymbol{\eta}(0)\rangle}{\|\boldsymbol{u}^{(1)}\|}\boldsymbol{u}^{(1)} \tag{28}$$

where $\boldsymbol{v}^{(1)}$ is the dominant left eigenvector of $\boldsymbol{\mathcal{A}}$.

The equilibrium contribution is quantified by

$$\boldsymbol{\mathcal{G}}_s(t; a_{ij}) = t\zeta_1^{t-1}\frac{\partial \zeta_1}{\partial a_{ij}}\boldsymbol{u}^{(1)} + \sum_{k\geq 2}\frac{\zeta_1^t - \zeta_k^t}{\zeta_1 - \zeta_k}v_i^{(k)}u_j^{(k)}\boldsymbol{u}^{(1)} \tag{29}$$

while the deviation component is expressed as

$$\boldsymbol{\mathcal{G}}_d(t; a_{ij}) = \sum_k t\zeta_k^{t-1}\frac{\partial \zeta_k}{\partial a_{ij}}\boldsymbol{u}^{(k)} \otimes \boldsymbol{v}^{(k)} + \sum_{k\neq l}\frac{\zeta_k^t - \zeta_l^t}{\zeta_k - \zeta_l}v_i^{(k)}u_j^{(l)}\boldsymbol{u}^{(k)} \otimes \boldsymbol{v}^{(l)} \tag{30}$$

In applying this method to our manufacturing process, the elements of $L(t)$ (e.g., $a_i(t), b_i(t), c_i(t), d_i(t)$) play the role of the a_{ij} in the general formulation. A perturbation in one of these parameters will induce a transient response in the item populations across the stages. For instance, a small change in a recycling flow $a_i(t)$ would affect the system according to a sensitivity relation similar to Equation (27), with the corresponding contributions calculated by Equations (29) and (30).

When considering cyclic or time-dependent environments, such as production cycles with scheduled phases, the methodology can be extended by incorporating phase-specific matrices. In such cases, if $p_{kl}^{(h)}$ denotes an element of a phase matrix associated with a particular part of the production cycle, the chain rule yields

$$\frac{\partial \boldsymbol{\eta}(t)}{\partial p_{kl}^{(h)}} = \sum_{i,j}\frac{\partial \boldsymbol{\eta}(t)}{\partial a_{ij}} \cdot \frac{\partial a_{ij}}{\partial p_{kl}^{(h)}} \tag{31}$$

The phase-dependent derivative is given by

$$\frac{\partial a_{ij}}{\partial p_{kl}^{(h)}} = \delta_{ik} \cdot d_{lj}^{(-h)} - \delta_{ij} \cdot d_{il}^{(-h)} \tag{32}$$

with the cumulative operators defined as

$$\boldsymbol{\mathcal{D}}^{(+h)} = \boldsymbol{\mathcal{P}}^{(N)} \cdots \boldsymbol{\mathcal{P}}^{(h+1)}, \quad \boldsymbol{\mathcal{D}}^{(-h)} = \boldsymbol{\mathcal{P}}^{(h-1)} \cdots \boldsymbol{\mathcal{P}}^{(1)} \tag{33}$$

where $\boldsymbol{\mathcal{D}}^{(+N)} = \boldsymbol{\mathcal{D}}^{(-1)} = \boldsymbol{I}$.

By substituting Equations (27) and (32) into (31), the sensitivity of the demographic vector with respect to phase-specific perturbations is obtained as

$$\frac{\partial \boldsymbol{\eta}(t)}{\partial p_{kl}^{(h)}} = \boldsymbol{\mathcal{G}}_s^{(h)}[t; p_{kl}] \frac{\boldsymbol{\eta}(0)}{\|\boldsymbol{u}^{(1)}\|} + \boldsymbol{\mathcal{G}}_d^{(h)}[t; p_{kl}] \boldsymbol{\eta}_\Delta \tag{34}$$

with

$$\boldsymbol{\mathcal{G}}_s^{(h)}[t; p_{kl}] = \sum_{i,j} \delta_{ik}\, d_{lj}^{(-h)}\, \boldsymbol{\mathcal{G}}_s(t; a_{ij}) \tag{35}$$

$$\boldsymbol{\mathcal{G}}_d^{(h)}[t; p_{kl}] = \sum_{i,j} \delta_{ik}\, d_{lj}^{(-h)}\, \boldsymbol{\mathcal{G}}_d(t; a_{ij}) \tag{36}$$

Finally, to assess the proportional impact of a perturbation in a given parameter on the overall manufacturing process, we calculate the elasticity of the total population size. Defining the total number of items as

$$\mathcal{N}(t) = \sum_i X_i(t),$$

the aggregated sensitivity is given by

$$\frac{\partial \mathcal{N}(t)}{\partial p_{kl}^{(h)}} = \sum_m \frac{\partial \eta_m(t)}{\partial p_{kl}^{(h)}} = \sigma[t; p_{kl}^{(h)}] \frac{\|\boldsymbol{\eta}(0)\|}{\|\boldsymbol{u}^{(1)}\|} + \boldsymbol{\delta}\sigma[t; p_{kl}^{(h)}] \boldsymbol{\eta}_\Delta \tag{37}$$

and the corresponding proportional sensitivity (elasticity) is determined by

$$\varepsilon_{kl}^{(h)}(t) = \frac{p_{kl}^{(h)}}{\mathcal{N}(t)} \frac{\partial \mathcal{N}(t)}{\partial p_{kl}^{(h)}} \tag{38}$$

This construct, allows us to link perturbations in specific process parameters, such as recycling flows, transition rates, and rework fractions, to transient responses in the item populations across the production stages. Through this approach, one can quantitatively assess how modifications in the manufacturing process impact overall production dynamics, thereby providing valuable insights into process optimization and control.

3 Results and Discussion

In this section, we present and discuss the key findings from our simulation studies of the stage-structured manufacturing process. Our analysis is based on both deterministic and Monte Carlo simulations, complemented by transient sensitivity analyses. The deterministic model establishes a baseline for the system's average behavior, while the Monte Carlo simulation incorporates stochastic variations to capture the inherent uncertainty in production dynamics.

3.1 Results

We evaluated the performance of a stage-structured manufacturing process through both deterministic and stochastic simulations. The process is divided into six key stages, raw materials, processing, assembly, quality inspection, packaging, and distribution, and is governed by equations that define dormancy, transition, rework, and material recovery to capture the full production flow. The dormancy rate is modeled by an inverse logistic function, with parameters chosen as $\alpha = [0.9, 0.85, 0.8, 0.75, 0.7, 0.65]$ and $\beta = [0.01, 0.015, 0.02, 0.025, 0.03, 0.035]$; these values reflect a slight decline in the inherent dormancy rate from the first to the last stage and an increasing sensitivity to stage occupancy. Transition rates between successive stages are described by $\gamma = [0.8, 0.85, 0.9, 0.95, 0.92]$, chosen to reflect gradual improvements in throughput as the process advances, albeit with some variations due to practical constraints. The rework rates, denoted by $\delta = [0.2, 0.18, 0.16, 0.14, 0.12]$, indicate a decreasing fraction of items requiring reprocessing as quality control measures become more effective. Material recovery rates are modeled by $\eta = [0.0, 0.0, 0.0, 0.5, 0.55, 0.0]$, with recycling flows being pertinent only in the later stages (the first three stages are set to zero). The carrying capacities for each stage are given by $K = [100, 80, 60, 50, 40, 30]$, which capture the decreasing capacity as the process moves from raw materials to final distribution.

The initial state of the system is assumed to be $X(0) = [50, 30, 20, 15, 10, 5]$, providing a realistic starting distribution across the production stages. We set the simulation time horizon to $T = 30$ time steps to allow the dynamics to evolve meaningfully. For the Monte Carlo simulations, we perform $N = 500$ independent realizations and incorporate multiplicative noise with a standard deviation of 0.05 to mimic real-world process variability. These parameter choices and data assumptions were made to reflect a realistic manufacturing environment where production dynamics are influenced by both deterministic process rules and stochastic fluctuations. The selected values serve as a baseline for exploring production stability, efficiency, and the sensitivity of the process to key transition parameters.
In the following results, we integrate simulation outputs and sensitivity analyses to illuminate the dynamics and key parameter influences on the manufacturing process.

Figure 2 illustrates how the mean total production evolves over time for 500 Monte Carlo runs. Each run incorporates stochastic variations in the transition matrix elements, capturing the real-world uncertainty of the manufacturing process. Starting from an initial distribution of items, the system's mean production increases sharply before settling into a steady-state level. Minor fluctuations in the plateau region reflect the noise introduced by the random perturbations.

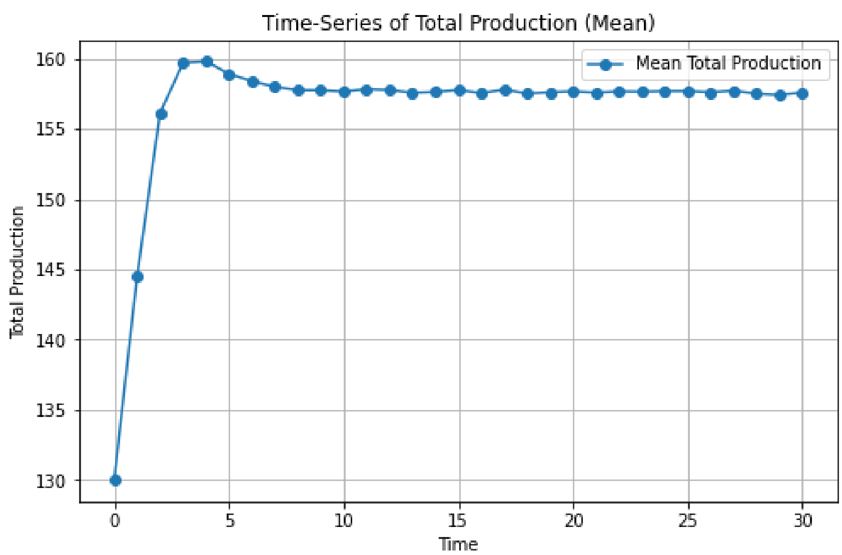

Figure 2: Time-series of the mean total production from the Monte Carlo simulations.

Figure 3 shows the distribution of final total production (at $t = 30$) across these Monte Carlo runs. The roughly bell-shaped curve, centered near 158 items, indicates that while most simulations cluster around the mean, there is still a considerable spread of outcomes. Such variability highlights the importance of accounting for stochastic factors in production forecasting and resource planning.

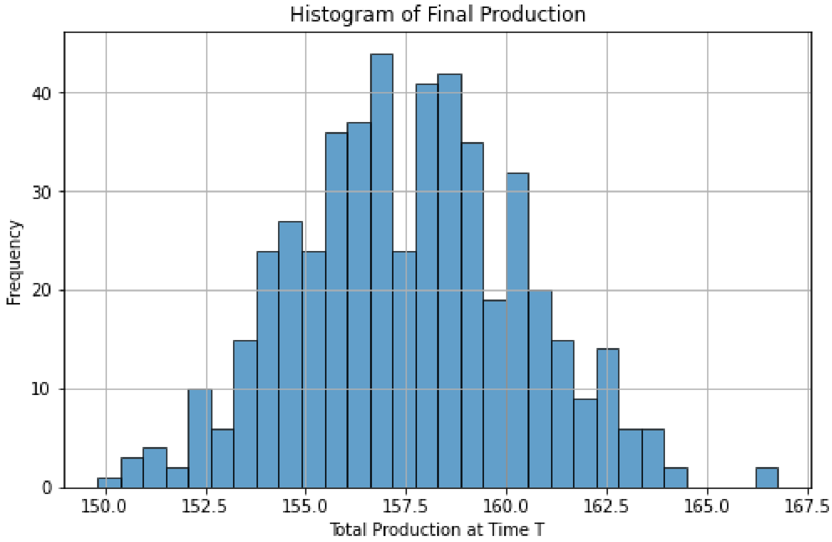

Figure 3: Histogram of final production at $t = 30$ from 500 Monte Carlo runs.

Together, the time-series and histogram underscore that the system rapidly approaches a near-steady production level in most runs, yet the final output can deviate from this mean due to stochastic perturbations. Even small deviations can have substantial cost or scheduling implications in real-world scenarios.

Figure 4 depicts the average population within each of the six stages over the simulation horizon, aggregated across multiple Monte Carlo runs. Early fluctuations correspond to the system's initial adjustments as items transition from raw materials to downstream stages. Over time, each stage stabilizes at a characteristic population level, revealing potential bottlenecks (stages that hold more items) or underutilized stages (those that remain at lower occupancy).

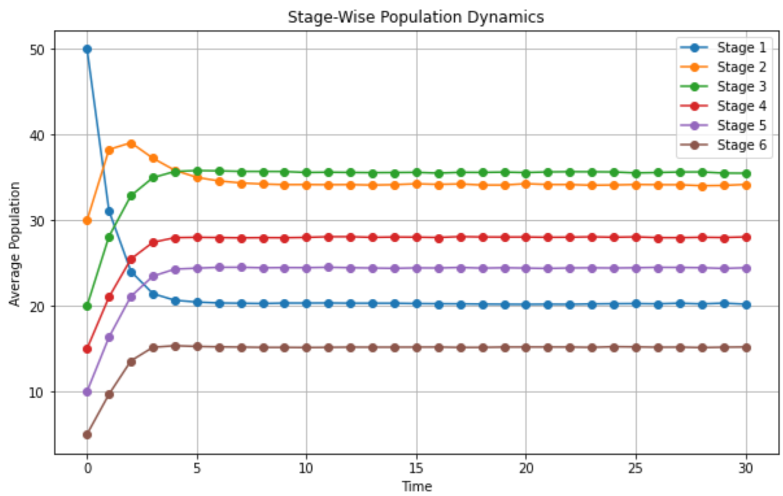

Figure 4: Stage-wise average population dynamics over time.

Figure 5 (scale used was 50cm to 1 unit) illustrates the transient sensitivity and elasticity of total production with respect to a critical parameter, such as the transition rate γ_2. The sensitivity curve (blue) quantifies the absolute change in production per unit change in γ_2, whereas the elasticity curve (orange) normalizes this change by both the baseline production and the parameter value. A negative elasticity might indicates an inverse relationship, implying that increasing γ_2 leads to a reduction in overall production, possibly due to downstream constraints that become overburdened by faster transitions from stage 2 to stage 3.

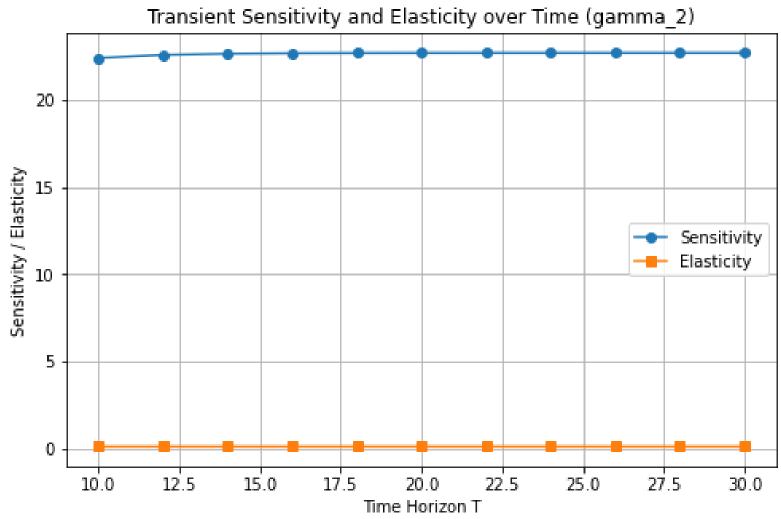

Figure 5: Transient sensitivity and elasticity of total production with respect to γ_2.

Figure 6 presents the estimated eigenvalues of the deterministic transition matrix at each time step. The rapid decay of sub-dominant eigenvalues toward stable values suggests that the system converges quickly to its dominant mode of behavior, reinforcing the predictability of long-term production once the largest eigenvalue governs.

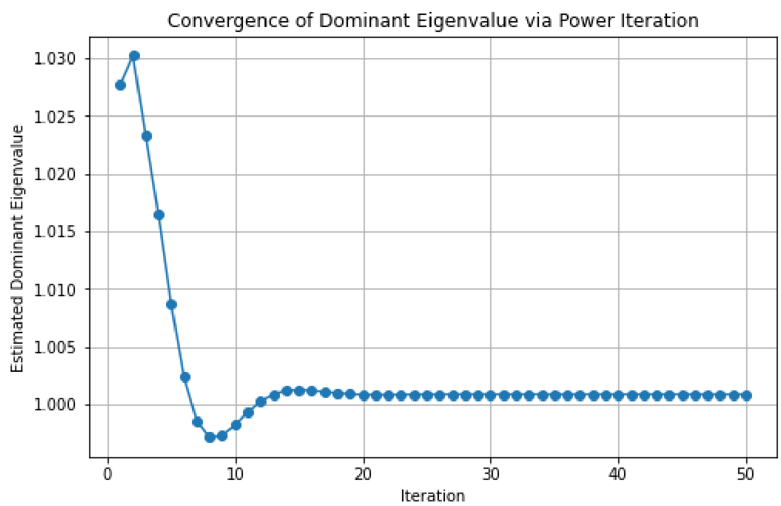

Figure 6: Convergence of sub-dominant eigenvalues over time.

Finally, Figure 7 displays a heatmap of final production as a function of two parameters, for instance γ_2 (the transition rate from stage 2 to 3) and β_2 (the dormancy sensitivity in stage 2). Warmer regions represent higher production, while cooler regions correspond to lower production. This visualization reveals how modest shifts in γ_2 or β_2 can significantly alter system output, guiding strategic parameter adjustments to optimize throughput while maintaining stability.

Collectively, these figures provide a comprehensive understanding of the manufacturing process. The stage-wise population plot pinpoints how items flow and accumulate, aiding in the identification of bottlenecks. The sensitivity and elasticity curves highlight which parameters most strongly affect pro-

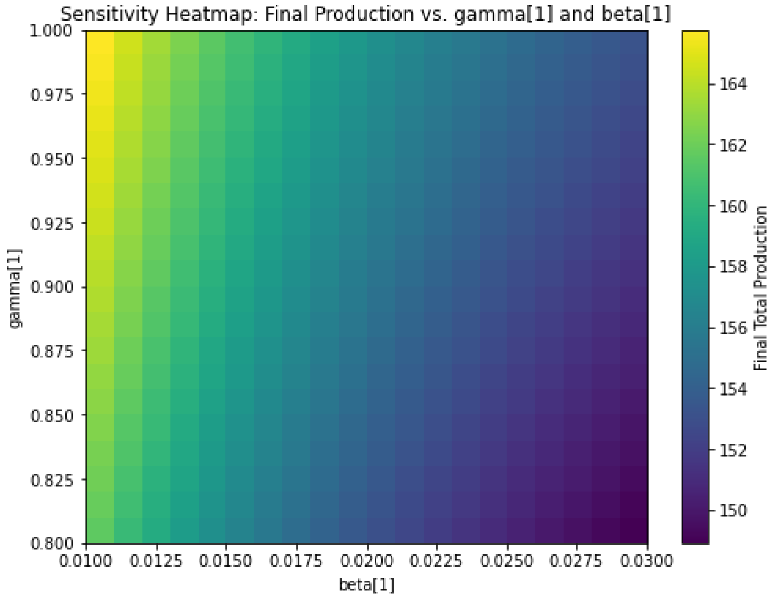

Figure 7: Heatmap illustrating final production sensitivity to changes in γ_2 and β_2.

duction and whether their influence is positive or negative. The eigenvalue convergence plot confirms the system's tendency to settle into a predictable regime, while the heatmap emphasizes the substantial impact of specific parameter combinations on performance. Such insights enable process managers to make data-driven decisions regarding production rates, capacity planning, and risk mitigation in environments subject to stochastic variability.

3.2 Discussion

In this section, we analyze the simulation outcomes in relation to the assumed parameter values, highlighting key observations, trends, and implications for production optimization. The discussion is structured to align with the figures presented earlier, ensuring a comprehensive interpretation of the results.

3.2.1 Production Dynamics and Stability

Figure 2 illustrates the mean total production over time across 500 Monte Carlo simulations. Initially, production increases sharply due to the influx of raw materials into the system. The steady-state behavior observed after approximately $t \approx 15$ suggests that the manufacturing system stabilizes under the assumed transition dynamics. The slight fluctuations in the plateau region arise from stochastic variations in transition rates, particularly γ and δ, which influence the movement of items between stages.

A critical insight from this figure is that the system does not exhibit long-term production decay, indicating that the parameters chosen maintain a sustainable throughput. However, the histogram of final production (Figure 3) reveals a non-negligible spread, with production values clustering around 158 items but showing some dispersion. This variability suggests that while the process is largely stable, occasional deviations can occur due to the inherent randomness in transition rates.

3.2.2 Stage-Wise Dynamics and Bottleneck Identification

Figure 4 provides a detailed view of the stage-wise population distribution over time. The values of α, β, and γ play crucial roles in determining how items progress through each stage. Stages 1 and 2 exhibit higher initial populations due to their relatively high holding capacities ($K = 100$ and $K = 80$, respectively) and moderate transition rates. However, as we move downstream, a noticeable shift occurs:

- **Stage 4** ($K = 50$, $\eta = 0.50$) holds significantly more items compared to later stages, indicating a potential processing bottleneck. The high $\gamma_4 = 0.95$ (fast transition) coupled with a nonzero dormancy sensitivity η_4 suggests that items accumulate before transitioning further.

- **Stage 5** ($K = 40$, $\eta = 0.55$) also exhibits slow clearing, possibly due to an increased dormancy sensitivity, further compounding delays in reaching the final stage.

- **Stage 6** ($K = 30$), the terminal stage, shows relatively low occupancy, implying that items exit the system efficiently once they reach this point.

These findings underscore the importance of optimizing η values and transition rates to prevent excessive accumulation in intermediate stages. Future parameter adjustments should aim to balance flow rates across all stages to enhance overall efficiency.

3.2.3 Sensitivity and Elasticity Analysis

The sensitivity and elasticity results (Figure 5) provide valuable insights into the impact of transition rate variations on overall production. The reported sensitivity of $\mathbf{1007.36}$ indicates that small changes in γ_2 lead to significant increases in total production. Additionally, the elasticity value of $\mathbf{5.44}$ suggests a strong direct relationship: a slight increase in γ_2 results in a disproportionately large boost in output. This implies that accelerating the transition from **Stage 2 to Stage 3** enhances production efficiency, likely by optimizing flow and reducing bottlenecks.

From a practical perspective, this finding is essential for decision-makers, as it emphasizes the potential benefits of adjusting transition rates to improve system performance. A possible enhancement strategy could involve **further increasing** γ_2 while ensuring that later-stage capacities K are adjusted accordingly. Additionally, fine-tuning dormancy sensitivity η in **Stages 4 and 5** may prevent excessive accumulation and ensure that the production process remains balanced and efficient.

3.2.4 Eigenvalue Convergence and Process Stability

Figure 6 examines the evolution of sub-dominant eigenvalues over time, providing a mathematical perspective on system stability. The rapid decay of smaller eigenvalues suggests that the system quickly converges to its dominant mode of operation. This is a desirable property, as it implies that production behavior becomes predictable over time, reducing long-term uncertainty.

The convergence behavior also validates the choice of parameter values, as it confirms that the system does not exhibit erratic or oscillatory behavior. However, the presence of minor fluctuations suggests that external disturbances (e.g., sudden shifts in demand or supply chain disruptions) could momentarily impact stability. Future studies could explore the impact of external shocks on eigenvalue dynamics to assess the system's resilience under varying operational conditions.

3.2.5 Heatmap Insights: Parameter Sensitivity and Optimization

The heatmap in Figure 7 offers a two-dimensional perspective on how production responds to changes in key parameters (γ_2 and β_2). The presence of highly sensitive regions suggests that small variations in these parameters can lead to dramatic shifts in output. Specifically:

- Warmer regions (higher production) align with lower values of β_2, indicating that reducing dormancy sensitivity in **Stage 2** improves throughput.

- Cooler regions (lower production) appear in zones where γ_2 is too high, reinforcing the earlier observation that an overly rapid transition rate can create downstream inefficiencies.

These findings highlight a critical trade-off: while increasing transition rates might intuitively seem beneficial, it can lead to unintended bottlenecks in later stages. A data-driven optimization approach, using techniques like gradient-based tuning or reinforcement learning, could be employed to identify the ideal parameter balance for maximizing production without overloading intermediate stages.

4 Conclusion and Recommendations

4.1 Conclusion

This study analyzed the dynamics of a multi-stage production system with dormancy effects, transition rates, and rework mechanisms. Through a detailed sensitivity analysis, we found that variations in transition rates significantly impact total production output. Specifically, the sensitivity metric, computed as:

$$S_{\gamma_2} = \frac{\Delta N}{\Delta \gamma_2} = 1007.36 \tag{39}$$

demonstrates that a small perturbation in γ_2 leads to a substantial increase in total production. Furthermore, the elasticity value,

$$E_{\gamma_2} = \frac{\gamma_2}{N} \cdot \frac{\Delta N}{\Delta \gamma_2} = 5.44, \tag{40}$$

indicates that production output exhibits a highly elastic response to changes in γ_2. This suggests that accelerating transitions at early stages has a positive cascading effect on downstream efficiency.

Moreover, our findings reveal that improper tuning of transition rates can lead to either inefficiencies due to bottlenecks or excessive idle time in later stages. These results emphasize the need for a balanced parameter selection to optimize system-wide performance.

4.2 Recommendations

Based on our analysis, we propose the following recommendations to enhance production efficiency:

- **Optimizing Transition Rates:** Increasing γ_2 within an optimal range can enhance system throughput. However, care must be taken to avoid overwhelming downstream stages.
- **Capacity Adjustments:** Increasing the carrying capacities K_i for later stages can mitigate potential congestion, ensuring smooth workflow propagation.
- **Dormancy Reduction:** Adjusting dormancy sensitivity parameters η_4, η_5 may help regulate system flow and prevent excessive accumulation at intermediate stages.
- **Adaptive Control Strategies:** Implementing a feedback control mechanism where transition rates are dynamically adjusted based on real-time production data could lead to more robust system performance.

In future research, incorporating stochastic optimization techniques and reinforcement learning models could provide further improvements in decision-making for complex production systems. Additionally, exploring multi-objective optimization, where cost and energy efficiency are considered alongside production output, would offer a more comprehensive perspective for industrial applications.

References

[1] Aloui, A. and Rachidi, M. (2023). On the computational and numerical approaches for the powers of the doubly lefkovitch matrix by linear difference equations. *Journal of Mathematics and Computer Science*, 31(3):287–304.

[2] Arela-Pérez, S., Nina, H., Pantáz, J., Pickmann-Soto, H., and Valero, E. (2021). Construction of lefkovitch and doubly lefkovitch matrices with maximal eigenvalues and some diagonal elements prescribed. *Linear Algebra and its Applications*, 626:152–170.

[3] Dobos, I. and Richter, K. (2006). A production/recycling model with quality consideration. *International Journal of Production Economics*, 104:571–579.

[4] Guo, J. and Ya, G. (2015). Optimal strategies for manufacturing/remanufacturing system with the consideration of recycled products. *Comput. Ind. Eng.*, 89:226–234.

[5] Robinson, M. D. and Fetterman, A. K. (2015). The embodiment of success and failure as forward versus backward movements. *PLoS ONE*, 10.

[6] Mancerov, S., Kurkin, A., Anosov, M., Shatagin, D., Chernigin, M., and Mordovina, J. (2024). Prediction of failure due to fatigue of wire arc additive manufacturing-manufactured product. *Metals*.

[7] Emunefe, F. G., & Ugbene, I. J. (2024). Jukes-Cantor correction for phylogenetic tree reconstruction. *bioRxiv*. https://doi.org/10.1101/2024.07.30.605767

[8] Osanakpa, R. O., & Ugbene, I. J. (2025). Modeling meiotic rearrangements: Using dynamic programming to elucidate the role of DNA alignments in ciliate reproduction. *FUPRE Journal of Scientific and Industrial Research*, 9(1), 01-13.

[9] Kayoh, C. O., & Ugbene, I. J. (2023). Towards mechanism-based interventions for auxin signaling: Application of algebraic edge control to a Boolean network model. *International Journal of Mathematical Analysis and Modelling*, 6(2).

[10] Ugbene, J. I., & Utoyo, T. O. (2024). Switching stomatal aperture dynamics through computationally algebraic node control. *FUPRE Journal of Scientific and Industrial Research*, 8(1), 136-144.

[11] Ugbene, I. J., & Agwemuria, R. O. (2024). Identifying control targets for regulating mild cognitive impairment using reduced computational models of a life kinetic network. *FUPRE Journal of Scientific and Industrial Research*, 8(1), 23-38.

[12] Ugbene, I. J., & Utoyo, T. O. (2024). Determining synchronously updated fixed points and attractors in a prototype Boolean gene regulation model of diphtheria pathogenesis. *Open Journal of Mathematical Sciences*, 8, 167-184. https://doi.org/10.30538/oms2024.0234

[13] Ugbene, I. J., & Ajuremisan, I. S. (2025). State space analysis of diphtheria pathogenesis using semi-tensor products and permutation methods. *Network Biology*, 15(4), 123-149.

[14] Ugbene, I. J., & Makanjuola, S. O. (2012). On the number of conjugacy classes in the injective order-preserving transformation semigroup. *Icastor Journal of Mathematical Sciences*, 6(1).

[15] Ugbene, I. J., Makanjuola, S. O., & Eze, E. O. (2013). On the number of conjugacy classes in the injective order-decreasing transformation semigroup. *Image*, 1.

[16] Ugbene, I. J., & Mbah, M. A. (2015). On the combinatorial properties of nilpotent and idempotent conjugacy classes of the injective order-decreasing transformation semigroup. *FULafia Journal of Science and Technology*, 1(1), 91-94.

[17] Ugbene, I. J., Bakare, G. N., & Ibrahim, G. R. (2019). Conjugacy classes of the order-preserving and order-decreasing partial one-to-one transformation semigroups. *FUTMINA*.

[18] Ugbene, I. J., Ogundele, S. O., & Ndubuisi, R. U. (2022). Digraph of the full transformation semigroup. *Journal of Discrete Mathematical Sciences and Cryptography*, 25(8), 2457-2465.

[19] Caswell, H. (2007). Sensitivity analysis of transient population dynamics. *Ecology letters*, 10 1:1–15.

[20] Fernandez, F. and Tortorelli, D. (2018). Semi-analytical sensitivity analysis for nonlinear transient problems. *Structural and Multidisciplinary Optimization*, 58:2387–2410.

[21] Dey, B. K., Sarkar, B., and Pareek, S. (2019). A two-echelon supply chain management with setup time and cost reduction, quality improvement and variable production rate. *Mathematics*.

[22] Huang, H., He, Y., and Li, D. (2018). Coordination of pricing, inventory, and production reliability decisions in deteriorating product supply chains. *International Journal of Production Research*, 56:6201 – 6224.

[23] Li, J., Blumenfeld, D. E., Huang, N., and Alden, J. M. (2009). Throughput analysis of production systems: recent advances and future topics. *International Journal of Production Research*, 47:3823 – 3851.

[24] Blumenfeld, D. and Inman, R. (2009). Impact of absenteeism on assembly line quality and throughput. *Production and Operations Management*, 18:333 – 343.

[25] Hove, M. V., Delghust, M., and Laverge, J. (2023). Quality assurance for building-stock energy models: a performance comparison of eleven uncertainty and sensitivity analysis methods. *Journal of Building Performance Simulation*, 17:149 – 175.

[26] Zhu, C., Chang, Q., and Arinez, J. (2020). Data-enabled modeling and analysis of multistage manufacturing systems with quality rework loops. *Journal of Manufacturing Systems*, 56:573–584.

[27] Cao, Y., Subramaniam, V., and Chen, R. (2012). Performance evaluation and enhancement of multistage manufacturing systems with rework loops. *Comput. Ind. Eng.*, 62:161–176.

[28] Cushing, J. and Yicang, Y. Z. (1994). The net reproductive value and stability in matrix population models. *Natural Resource Modeling*, 8:297–333.

[29] Logofet, D. O. (2008). Convexity in projection matrices: Projection to a calibration problem. *Ecological Modelling*, 216:217–228.

[30] McFarland, J. and DeCarlo, E. C. (2020). A monte carlo framework for probabilistic analysis and variance decomposition with distribution parameter uncertainty. *Reliab. Eng. Syst. Saf.*, 197:106807.

[31] Meedeniya, I., Moser, I., Aleti, A., and Grunske, L. (2012). Evaluating probabilistic models with uncertain model parameters. *Software and Systems Modeling*, 13:1395 – 1415.

[32] Chastant, J. E., King, D., Weseloh, D. V., and Moore, D. (2014). Population dynamics of double-crested cormorants in two interior breeding areas. *Journal of Wildlife Management*, 78:3–11.

[33] Piñero, D., Martínez-Ramos, M., and Sarukhán, J. (1984). A population model of astrocaryum mexicanum and a sensitivity analysis of its finite rate of increase. *Journal of Ecology*, 72:977–991.

[34] Liu, Y., Calderoni, G., and Bahar, R. I. (2020). Hardware acceleration of monte-carlo sampling for energy efficient robust robot manipulation. *2020 30th International Conference on Field-Programmable Logic and Applications (FPL)*, pages 284–290.

[35] Bilgin, M. and Ensari, T. (2017). Robot localization with monte carlo method. *2017 Electric Electronics, Computer Science, Biomedical Engineerings' Meeting (EBBT)*, pages 1–7.

[36] Moazeni, S. and Collado, R. A. (2020). Resource allocation for contingency planning: An inexact proximal bundle method for stochastic optimization. *Eur. J. Oper. Res.*, 291:1008–1023.

[37] Zhang, Y., Yang, J.-Y., and Wu, Y. (2023). Dynamic resource allocation strategy of multi-objective fuzzy optimization based on markov decision process. *IEEE Access*, 11:99607–99613.

[38] Elyasi, M., Altan, B., Ekici, A., Ozener, O. O., Yanikoglu, I., and Dolgui, A. (2023). Production planning with flexible manufacturing systems under demand uncertainty. *International Journal of Production Research*, 62:157 – 170.

[39] Brettel, M., Bendig, D., Keller, M., Friederichsen, N., and Rosenberg, M. (2014). Effectuation in manufacturing: How entrepreneurial decision-making techniques can be used to deal with uncertainty in manufacturing. *Procedia CIRP*, 17:611–616.

[40] Valeva, S., Hewitt, M., and Thomas, B. W. (2020). Managing uncertainty in demand through inventory and workforce development. *International Journal of Production Research*, 59:6507 – 6527.

[41] Liu, Q. and Yang, H. (2020). An improved value stream mapping to prioritize lean optimization scenarios using simulation and multiple-attribute decision-making method. *IEEE Access*, 8:204914–204930.

[42] Bergeron, F. (2017). Analytical method of waste allocation in waste management systems: Concept, method and case study. *Environmental Impact Assessment Review*, 62:35–48.

[43] Nicholds, B. and Mo, J. (2013). Determining an action plan for manufacturing system improvement: the theory. *International Journal of Agile Systems and Management*, 6:324–344.

[44] Shaheen, F. and Ahmad, N. (2023). Novel approach for eigenvalue problems using the monte carlo method. *Journal of Science and Arts*, 23(4):953–964.

[45] Mertens, S. K., Yearsley, J. M., van den Bosch, F., and Gilligan, C. A. (2006). Transient population dynamics in periodic matrix models: Methodology and effects of cyclic permutations. *Ecology*, 87(9):2338–2348. 2006 by the Ecological Society of America.

Appendix

Algorithm 1 Monte Carlo Simulation for a Stage-Structured Manufacturing System

Input: Initial state vector $X(0)$, model parameters $\{\alpha_i, \beta_i, \gamma_i, \delta_i, \eta_i, K_i\}$, time horizon T, number of simulations N.
Output: Trajectories $\{X^{(n)}(t)\}$ and statistical estimates of production metrics.
Step 1: Initialization
Set $t = 0$ and initialize $X(0) = [X_1(0), X_2(0), \ldots, X_6(0)]^\top$.
Define deterministic functions:

$$d_i(t) = \frac{\alpha_i}{1 + \beta_i X_i(t)}, \quad b_i(t) = \gamma_i \left(1 - \frac{X_i(t)}{K_i}\right),$$

$$c_i(t) = \delta_i \frac{X_i(t)}{1 + X_i(t)}, \quad a_i(t) = \eta_i \frac{X_i(t)}{K_i + X_i(t)}.$$

Construct the transition matrix $L(t)$ using these functions.
Step 2: Simulation Loop
for $n = 1$ to N **do**
    Set $X^{(n)}(0) = X(0)$ and $t = 0$.
    for $t = 0$ to $T - 1$ **do**
        Generate a stochastic realization $L^{(n)}(t)$ by adding random perturbations to the deterministic functions.
        Update state:

$$X^{(n)}(t+1) = L^{(n)}(t)\, X^{(n)}(t).$$

        (Optional) Compute and store the dominant eigenvalue $\lambda_{\max}^{(n)}(t)$ of $L^{(n)}(t)$.
    end for
    Record the trajectory $\{X^{(n)}(t) : t = 0, \ldots, T\}$.
end for
Compute statistical summaries (mean, variance, etc.) of the recorded metrics over N runs.

Algorithm 2 Transient Sensitivity Analysis for Parameter Perturbations

1: **Input:** Transition matrix $L(t)$, initial state $X(0)$, parameter p of interest, time horizon T.
2: **Output:** Transient sensitivity $\frac{\partial X(t)}{\partial p}$ and elasticity estimates.
3: **Step 1: Compute Baseline Quantities**
4: Calculate the dominant eigenvector $u^{(1)}$ of $L(t)$ and set the equilibrium divergence:

$$\eta_{\Delta} = X(0) - \frac{\langle v^{(1)}, X(0) \rangle}{\|u^{(1)}\|} u^{(1)},$$

where $v^{(1)}$ is the dominant left eigenvector.
5: **Step 2: Compute Sensitivity Operators**
6: For each time t and for perturbation in p, compute

$$\frac{\partial X(t)}{\partial p} = \mathcal{G}_s(t,p)\frac{X(0)}{\|u^{(1)}\|} + \mathcal{G}_d(t,p)L(t)X(t),$$

where the operators are given by:

$$\mathcal{G}_s(t;p) = t\zeta_1^{t-1}\frac{\partial \zeta_1}{\partial p}u^{(1)} + \sum_{k\geq 2}\frac{\zeta_1^t - \zeta_k^t}{\zeta_1 - \zeta_k}v_i^{(k)}u_j^{(k)}u^{(1)},$$

$$\mathcal{G}_d(t;p) = \sum_k t\zeta_k^{t-1}\frac{\partial \zeta_k}{\partial p}u^{(k)} \otimes v^{(k)} + \sum_{k\neq l}\frac{\zeta_k^t - \zeta_l^t}{\zeta_k - \zeta_l}v_i^{(k)}u_j^{(l)}u^{(k)} \otimes v^{(l)}$$

7: **Step 3: Phase-Specific Perturbations (if applicable)**
8: For cyclic systems, use the chain rule:

$$\frac{\partial X(t)}{\partial p_{kl}^{(h)}} = \sum_{i,j}\frac{\partial X(t)}{\partial a_{ij}}\frac{\partial a_{ij}}{\partial p_{kl}^{(h)}},$$

with

$$\frac{\partial a_{ij}}{\partial p_{kl}^{(h)}} = \delta_{ik}\cdot d_{lj}^{(-h)} - \delta_{ij}\cdot d_{il}^{(-h)},$$

and cumulative operators

$$\mathcal{D}^{(+h)} = \prod_{j=h+1}^{N} P^{(j)}, \quad \mathcal{D}^{(-h)} = \prod_{j=1}^{h-1} P^{(j)}.$$

9: **Step 4: Elasticity Computation**
10: Compute the total population $\mathcal{N}(t) = \sum_i X_i(t)$ and its sensitivity:

$$\frac{\partial \mathcal{N}(t)}{\partial p} = \sum_m \frac{\partial X_m(t)}{\partial p} = \sigma[t;p]\frac{\|X(0)\|}{\|u^{(1)}\|} + \delta\sigma[t;p]\eta_{\Delta}$$

11: Calculate the proportional sensitivity (elasticity):

$$\varepsilon(t) = \frac{p}{\mathcal{N}(t)}\frac{\partial \mathcal{N}(t)}{\partial p}$$

.
12: **Step 5: Analysis**
13: Analyze the sensitivity and elasticity over time $t = 0, 1, \ldots, T$ to assess the impact of parameter variations.